



# **Dual Ion Spectrometers and Their Calibration for the Fast Plasma Investigation on NASA's Magnetospheric Multiscale Mission**

*V.N. Coffey and M.O. Chandler  
Marshall Space Flight Center, Huntsville, Alabama*

## **The NASA STI Program...in Profile**

Since its founding, NASA has been dedicated to the advancement of aeronautics and space science. The NASA Scientific and Technical Information (STI) Program Office plays a key part in helping NASA maintain this important role.

The NASA STI Program Office is operated by Langley Research Center, the lead center for NASA's scientific and technical information. The NASA STI Program Office provides access to the NASA STI Database, the largest collection of aeronautical and space science STI in the world. The Program Office is also NASA's institutional mechanism for disseminating the results of its research and development activities. These results are published by NASA in the NASA STI Report Series, which includes the following report types:

- **TECHNICAL PUBLICATION.** Reports of completed research or a major significant phase of research that present the results of NASA programs and include extensive data or theoretical analysis. Includes compilations of significant scientific and technical data and information deemed to be of continuing reference value. NASA's counterpart of peer-reviewed formal professional papers but has less stringent limitations on manuscript length and extent of graphic presentations.
- **TECHNICAL MEMORANDUM.** Scientific and technical findings that are preliminary or of specialized interest, e.g., quick release reports, working papers, and bibliographies that contain minimal annotation. Does not contain extensive analysis.
- **CONTRACTOR REPORT.** Scientific and technical findings by NASA-sponsored contractors and grantees.
- **CONFERENCE PUBLICATION.** Collected papers from scientific and technical conferences, symposia, seminars, or other meetings sponsored or cosponsored by NASA.
- **SPECIAL PUBLICATION.** Scientific, technical, or historical information from NASA programs, projects, and mission, often concerned with subjects having substantial public interest.
- **TECHNICAL TRANSLATION.** English-language translations of foreign scientific and technical material pertinent to NASA's mission.

Specialized services that complement the STI Program Office's diverse offerings include creating custom thesauri, building customized databases, organizing and publishing research results...even providing videos.

For more information about the NASA STI Program Office, see the following:

- Access the NASA STI program home page at [<http://www.sti.nasa.gov>](http://www.sti.nasa.gov)
- E-mail your question via the Internet to [<help@sti.nasa.gov>](mailto:help@sti.nasa.gov)
- Phone the NASA STI Help Desk at 757-864-9658
- Write to:  
NASA STI Information Desk  
Mail Stop 148  
NASA Langley Research Center  
Hampton, VA 23681-2199, USA



# **Dual Ion Spectrometers and Their Calibration for the Fast Plasma Investigation on NASA's Magnetospheric Multiscale Mission**

*V.N. Coffey and M.O. Chandler  
Marshall Space Flight Center, Huntsville, Alabama*

National Aeronautics and  
Space Administration

Marshall Space Flight Center • Huntsville, Alabama 35812

---

***April 2017***

## **Acknowledgments**

The authors would like to express appreciation to C.J. Pollock (retired from Goddard Space Flight Center (GSFC)), Denali Scientific, LLC; L.A. Avanov, University of Maryland/Goddard Space Flight Center; and A. Diekmann, Jacobs ESSSA Group, Marshall Space Flight Center, for their continued support during the dual ion spectrometer calibration task. Thanks also goes to Y. Saito, Institute of Space and Astronautical Science, and D.J. Gershmann, University of Maryland/GSFC, for their editorial reviews.

This work was supported by the Magnetospheric Multiscale Mission under WBS 943396.05.03.02.08.02 for the Fast Plasma Investigation.

Available from:

NASA STI Information Desk  
Mail Stop 148  
NASA Langley Research Center  
Hampton, VA 23681-2199, USA  
757-864-9658

This report is also available in electronic form at  
<<http://www.sti.nasa.gov>>

## TABLE OF CONTENTS

1. INTRODUCTION .....	1
2. CALIBRATION SYSTEM AND APPROACH .....	2
3. CALIBRATION FACILITY .....	4
4. CALIBRATION PROCEDURES .....	7
4.1 Detector Characterization .....	8
4.2 Energy-Azimuth Angle and Polar Angle Response .....	9
5. SUMMARY RESULTS .....	14
5.1 Variation Across Deflection States .....	14
5.2 Variation Across Energy/Charge .....	14
6. CONCLUSIONS AND LESSONS LEARNED .....	16
REFERENCES .....	17

## LIST OF FIGURES

1.	The DIS ETU in the calibration chamber at MSFC. The automated RPA assembly is shown near the top. The RPA can be swung out, allowing beam access from above to the DIS entrance aperture, shown here above DIS sensor 0 .....	6
2.	Example real-time plot from DIS FM14, sensor 0 detector characterization procedure for operation point determinations. The signal and crosstalk count rates are shown for 20 threshold voltages at each of 6 MCP voltages .....	8
3.	Example of an annotated output plot from the polar angle response procedure for DIS FM04 sensor 1. Panel (a) is plotted in real-time and shows the 16-pixel response of count rate over the full polar angle FOV at the azimuth (deflected) angle of $-16.875^\circ$ . The lines are color coded according to pixel number. Panel (b) is plotted at the completion of the procedure documenting the centroid (right axis) and BCW (left axis) for each pixel's polar angle bandpass as shown in panel (a) .....	10
4.	Near real-time graphical and tabular output from the energy-azimuth angle procedure of 250 eV in the case of DIS FM16, sensor 1, pixel 2. Panel (a) shows the 2D energy-azimuth angle count rate response at five deflection states at the nominally centered angles of $-16.875^\circ$ , $-5.625^\circ$ , $0^\circ$ , $5.625^\circ$ , and $16.875^\circ$ . The horizontal axis label of instrument elevation translates to spacecraft azimuth. Panel (b) shows the 1D azimuth responses, and panel (c) shows the 1D energy ( $V_{ESA}$ ) responses. The curves in panels (b) and (c) are color coded according to the deflection state along with the response widths and centroids that are annotated on the right. Also shown are the derived values of the geometric factor, the effective area ( $A_{eff}$ ), polar angle width ( $dAz$ ), azimuth angle width ( $dE1$ ), and energy resolution ( $dE/E$ ) for each deflected state. The response centered near $-16.875^\circ$ is cut off at higher angles due to a hardware limit in the chamber and so gives artificially smaller performance values .....	13

## LIST OF TABLES

1.	Performance requirements .....	3
2.	Calibration measured performance .....	14

## LIST OF ACRONYMS

ABM	absolute beam monitor
BCW	box-car-width (bandpass)
CPT	comprehensive performance test
DIS	duel ion spectrometer
ESA	electrostatic analyzer
FOV	field of view
FPI	fast plasma investigation
FWHM	full width at half maximum
GSE	ground support equipment
ISAS	Institute of Space and Astronautical Science
LPT	limited performance test
MCP	microchannel plates
MSFC	Marshall Space Flight Center
RPA	retarding potential analyzer
UV	ultraviolet

## NOMENCLATURE

$A_{eff}$	effective aperture area
$dAz$	instrument polar angle bandpass
$dEl$	instrument azimuth bandpass
$dE/E$ or $\delta\epsilon/\epsilon$	energy bandpass
$E/q$	energy per charge
$eV/q$	electron volts per charge
$eV/V$	analyzer constant
$GF$	geometric factor
$V$	voltage



## TECHNICAL PUBLICATION

### **DUAL ION SPECTROMETERS AND THEIR CALIBRATION FOR THE FAST PLASMA INVESTIGATION ON NASA'S MAGNETOSPHERIC MULTISCALE MISSION**

#### **1. INTRODUCTION**

The 16 dual ion spectrometers (DISs) that make up the fast plasma investigation (FPI) instrument suite are dual-capped hemispheres mounted top to top with each allowing field-of-view (FOV) measurements over  $180^\circ$  in instrument azimuth (spacecraft polar). Each DIS electrostatic analyzer (ESA) was based on a toroidal capped hemisphere design as first suggested by Young et al.<sup>1</sup> The instruments also have annular deflection electrodes allowing the electrostatic FOV sweep over the range of  $45^\circ$  in instrument elevation (spacecraft azimuth). An overview of the FPI DIS is given in Pollock et al.<sup>2</sup>

The dual ion spectrometers were built by Meisei Electric in Gunma, Japan, under the direction of the Institute of Space and Astronautical Sciences (ISAS), a part of the Japanese Aerospace Exploration Agency. In addition to the numerical ray tracing to confirm the DIS measurement requirements, ISAS conducted two additional design studies mentioned here due to their importance to calibration and performance. Upon completion of a photon ray-tracing study along with chamber testing, the DIS design included serrated ESA surfaces that were blackened with a copper sulfide coating process. Using a Lyman alpha (proxy) ultraviolet (UV) source, ISAS characterized the UV susceptibility of all the flight units during functional testing, confirming the reduction of UV flux to a level of less than one count due to UV photons per sample period.

The DIS electrostatic deflectors are located close to the sensor apertures, so to prevent high voltage potential leakage to the external environment, a structure of two grids spaced 5 mm apart was designed for the aperture grid. Results from a static field simulation showed the double grid structure effectively reduced the leakage to a level low enough to meet the 1 V maximum surface voltage requirement, with a combined particle transmission of 81% (each grid of 90% transmission). Detailed discussion and figures for the optic designs of both the UV rejection and aperture structure are in Pollock et al.<sup>2</sup> For pre- and post-environmental beam testing, ISAS also conducted functional tests at 2 keV and 8 keV to determine performance responses from discriminator threshold, energy-azimuth angle, and polar angle response procedures.

## 2. CALIBRATION SYSTEM AND APPROACH

The FPI calibration strategy includes two main categories of measurements—those performed on the ground prior to launch and those performed in flight by exploiting the plasma environment and the capabilities of the other Magnetospheric Multiscale instrument suites. As part of the FPI instrument suite, the main objective of the DIS ground calibration approach was to obtain a full understanding of its response by measuring each spectrometer’s geometric factor and the end-to-end response over the range of look directions and energies while excited with a particle beam. Second, the measurements from a comprehensive calibration document the characteristics of the optics, high-voltage stepper supplies, and the detection system at a sufficient accuracy and fidelity to allow for the reduction of flight data into the physical quantities required to meet the science objectives and continuous flight calibration. In this Technical Publication the DIS ground testing and calibration approach, the calibration facility, the primary procedures with the resulting measurements along with their synoptic results, and lessons learned are discussed.

Due to the large number of sensors ( $16 \times 2$ ) and the tight schedule, the optimized calibration had to be methodical, efficient, and automated to every extent possible. Therefore, prior to the task, an efficiency study was conducted, accumulating accurate timings for various energy and 2D rotation angle resolution maps in an effort to determine the most extensive calibration possible given the time constraints and the mission requirements. The result of this study supported the calibration levels performed for the DIS units—the exhaustive and standard level. The exhaustive calibration was conducted for one instrument of each spacecraft suite and the standard calibration was performed on the remaining three instruments of each suite. In the case of the DIS, the exhaustive level differed mainly from the standard level in that each pixel sample was conducted with a greater number of beam energies.

With no delay between the instrument arrivals, an emphasis was placed on the full automation for every test procedure. This also included the completed analysis and documentation resulting from each procedure to be delivered to the FPI team every 24 hours. This approach was accomplished through the automated real-time software synchronization between three functions: the instrument ground support equipment (GSE) software, the chamber or laboratory control software, and the data analysis software. In real-time, the GSE and chamber control software synchronized and transferred the information from each instrument sweep table and chamber parameter to the data analysis software for immediate viewing of the response and analysis. This approach allowed the analyzed parameters to be quickly compared to the mission requirements (table 1) and for any performance issues to come to light quickly before the next instrument’s calibration start. This fully automated conveyor belt approach for charged-particle flight units with its real-time analysis and delivery made this calibration different than others known to date.

Table 1. Performance requirements.

Dual Ion Sensors	Requirement
Pixel geometric factor	$\geq 5 \times 10^{-4} \text{ cm}^2\text{-sr-eV/eV}$
Particle energy measurement range	10 eV – 30 keV
Energy $\Delta E/E$ FWHM resolution	$\leq 20\%$
Instrument elevation or spacecraft azimuth angle deflected FOV	$\pm 17^\circ$
Instrument elevation or spacecraft azimuth angle FWHM resolution	$\leq 11.25^\circ$
Instrument azimuth or spacecraft polar angle instantaneous FOV	$180^\circ$
Instrument azimuth or spacecraft polar angle FWHM resolution	$\leq 15^\circ$
Temporal resolution	150 ms

### 3. CALIBRATION FACILITY

The DIS flight units were tested and calibrated in the Low Energy Electron and Ion Facility at NASA Marshall Space Flight Center (MSFC). It is a heritage calibration laboratory designed for the testing and calibration of particle detectors over their complete range of particle energy, mass, flux, and angular acceptance. Some of its systems are listed below that were needed for the tight schedule and tight intracalibration requirements between the 16 DIS dual-sensor flight units:

(1) A large oil-free vacuum chamber to accommodate the large size of the DIS unit at the largest angle rotation needed for measurements over the full instrument response. Chamber pressures quickly reaching less than  $1.4 \times 10^{-5}$  Pa ( $1 \times 10^{-7}$  Torr) within a couple of hours allowing the start of the 24-hour maximum pressure requirement.

(2) A single, spatially broad ion source providing the energy per charge ( $E/q$ ) range from less than 10 eV through 35 keV with an monoenergetic and monodirectional steady flux ranging from  $10^3$  to  $10^8$  cm<sup>-2</sup>s<sup>-1</sup>. The tight schedule drove a need for one particle source that was capable of the full energy range. Prior to the calibration task, this source was tested and documented with respect to its performance on energy and flux stability, temperature width, flux range, and spatial uniformity.

(3) An automated DIS support fixture and rotation system providing 2D orthogonal angle rotations and the rotation from one sensor head to another. A system of inclinometers providing independent angle measurements with respect to the gravity vector within  $\pm 0.2^\circ$  accuracy.

(4) Ion source diagnostics using a large segmented retarding potential analyzer (RPA) capable of at least 4.5 keV and mounted on a rotation arm. An automated RPA rotation arm, beam current-voltage sweep with analysis providing real-time documentation of the beam's energy, temperature width, and current density at designated times within the procedures.

(5) GSE with software for the DIS control, data acquisition, and calibration synchronization commands. The housekeeping parameters and raw DIS count data are displayed in real-time to monitor the health of the instrument.

(6) Chamber control command, data acquisition, and monitoring software for the systems: rotations, inclinometers, chamber pressure, RPA motion, and RPA current-voltage sweep with analysis.

(7) Analysis software to ingest the GSE data and chamber control data for real-time viewing of the responses with analysis, then concluding with the final analysis of the derived parameters, generation of the final plots, and archival of data at the completion of the procedure.

The ion source beam is broad and produces ions by electron impact ionization and accelerates them electrostatically to the commanded  $E/q$ . The optic design is based on Biddle et al.<sup>3</sup> and was redesigned for higher voltage operation in preparation for DIS calibration to enable the generation of ion beams with energies up to 40 keV/ $q$ . The anode is controlled through the option of five power supplies each with 16-bit resolution with the voltage output controlled through a continuous feedback 1-s command loop. Typical DIS operating current densities were near 0.05 pA/cm<sup>2</sup> during calibration. Other ranges of current densities were available and utilized during selected procedures. RPA results show that the ion beam temperatures ranged from <1% of drift energy at 3 keV to 30% at 10 eV. The composition of the calibration beam is determined by the composition of the gas bled into the source. Molecular nitrogen gas was used to calibrate all 16 DIS flight instruments.

Prior to calibration, the ion source optics and RPA diagnostics were validated using a cylindrical ESA of 30 keV/ $q$  with a 0.5% energy and 0.25° angle resolution.<sup>4</sup> Two RPAs were also utilized—a smaller and larger analyzer with  $E/q$  maximum capabilities of 1.5 keV and 4.5 keV, respectively. Tests were conducted over the overlapping energy ranges with each device simultaneously to calibrate the ion source's admitted particle energy and confirm agreement between the devices over the full range of the DIS. Further, during the calibration of DIS FM10, the beam flux measured by the RPA was cross-calibrated against that measured by an absolute beam monitor (ABM)<sup>5</sup> provided by Southwest Research Institute. The beam fluxes measured by the RPA and the ABM device agreed to within 10% within the allowable flux range.

The beam energy and flux are determined from RPA curves, using the RPA rotated into the beam approximately 15 cm above the DIS aperture. Figure 1 is a photo of a DIS unit mounted in the chamber. The RPA curves of the beam current plotted as a function of the RPA voltage ( $V_{\text{RPA}}$ ) are obtained after the beam energy and current ( $V_{\text{RPA}} = 0$ ) is observed to be highly stable and before execution of the procedure. The beam  $E/q$  and temperature width is determined by fitting a Gaussian function to the negative first derivative of the RPA curve. Thereafter, the RPA is automatically rotated into the beam in the middle and end of each procedure and the beam current measured ( $V_{\text{RPA}} = 0$ ) and recorded with the other chamber controls. The mean value of these three measurements is used in combination with the Faraday Cup effective area of 2.99 cm<sup>2</sup> to compute the beam flux of record.

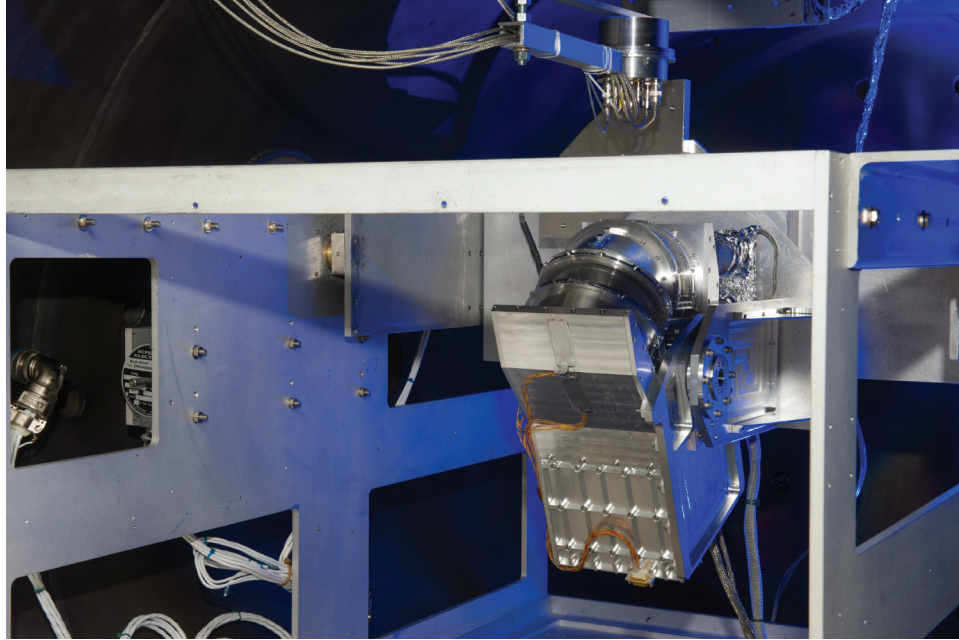


Figure 1. The DIS ETU in the calibration chamber at MSFC. The automated RPA assembly is shown near the top. The RPA can be swung out, allowing beam access from above to the DIS entrance aperture, shown here above DIS sensor 0.

#### 4. CALIBRATION PROCEDURES

Five main procedures were conducted for each DIS sensor as part of its calibration. Prior to these, a limited performance test (LPT) was conducted before pumping followed by a comprehensive performance test (CPT) after the chamber pressure requirements were met. The LPT and CPT were automated scripts executed from the GSE software. Depending on the script, the software checked all of the instrument's currents and temperatures, low and high range voltage commanding and monitor outputs, voltage step timings, stability and noise, read and write registers, etc. Upon completion, an executive summary along with the output documentation files were distributed and archived.

The primary aspects of three of the automated procedures are described here with any differing specifics described within each section. In general, the chamber control software mechanically stepped the DIS aperture through a 2D rotation matrix through both the polar angle FOV and azimuth (deflected) angle FOV. The resolution of the two angle dimensions depended on the procedure and the performance parameter being measured. An inclinometer system confirmed each angle within  $\pm 0.2^\circ$  before the next action of the procedure. After each completed rotation step in the matrix, a stepper table from the instrument's GSE software was executed. The stepper table was tailored for each particle beam's  $E/q$ , stepping through the appropriate  $V_{\text{ESA}}$  and  $V_{\text{DEF}}$  voltage combination for each of five deflected angle states:  $\pm 16.865^\circ$ ,  $\pm 5.625^\circ$ , and  $0^\circ$  and wide enough to capture the entire  $V_{\text{ESA}}/V_{\text{DEF}}$  bandpass. The  $V_{\text{DEF}}$  voltage was set at the ratio of 0.85 and 0.27 of  $V_{\text{ESA}}$  for the larger and smaller angle states, respectively. Four identical sweep tables made up each stepper table. Real-time monitoring of the respective parameters from each of the three software functions were continuously displayed from start to completion.

The end of each procedure, marked by the completion of the 2D rotation matrix, resulted in the creation of 2D  $V_{\text{ESA}}/V_{\text{DEF}}$  count rate maps for each angle step of the rotation matrix. Immediately upon completion (within a second or two), the annotated PDF plot was displayed with the analyzed performance parameters. All files and annotated plots were then archived and collected for distribution each night to the FPI team for study.

In addition to the three primary procedures described below, there were two additional procedures used to complete the sensor characterization that were executed in a similar manner but with the execution of the in-flight stepper table. One characterized the timing response with the required 1 ms integration period over the full  $V_{\text{ESA}}/V_{\text{DEF}}$  voltage range over the polar angle FOV. The other characterized the dark counts for each pixel with no particle beam illumination. Another important component of calibration was determining the precision of the  $V_{\text{ESA}}/V_{\text{DEF}}$  stepper voltages over their full voltage and temperature range with this being conducted for two of the flight units.



#### 4.1 Detector Characterization

The DIS performance in space is strongly dependent upon the operating voltages of the microchannel plates (MCPs) stack and the A121 charge sensitive preamplifier's discriminator threshold (hereafter referred to as threshold). Each DIS detector was characterized for this operating point through a nested loop of 20 threshold voltages at each of six MCP voltages while making measurements of the count rate at the 16 ( $\times 2$ ) illuminated pixels. This procedure was conducted by mechanically stepping the DIS through the centered 16 pixels across the polar angle FOV along with the synchronized commanded execution of the appropriate  $V_{\text{ESA}}/V_{\text{DEF}=0}$  stepper table for the input particle energy for each of the  $V_{\text{MCP}}/V_{\text{threshold}}$  values. Each data point, plotted in real-time, characterized the completed curves that determined the operating MCP stack and threshold voltage (fig. 2). They also characterized the pixel-to-pixel MCP efficiency variation, crosstalk, signal loss due to MCP gain variation, and noise level. Further discussion is in Gliese et al.<sup>6</sup>

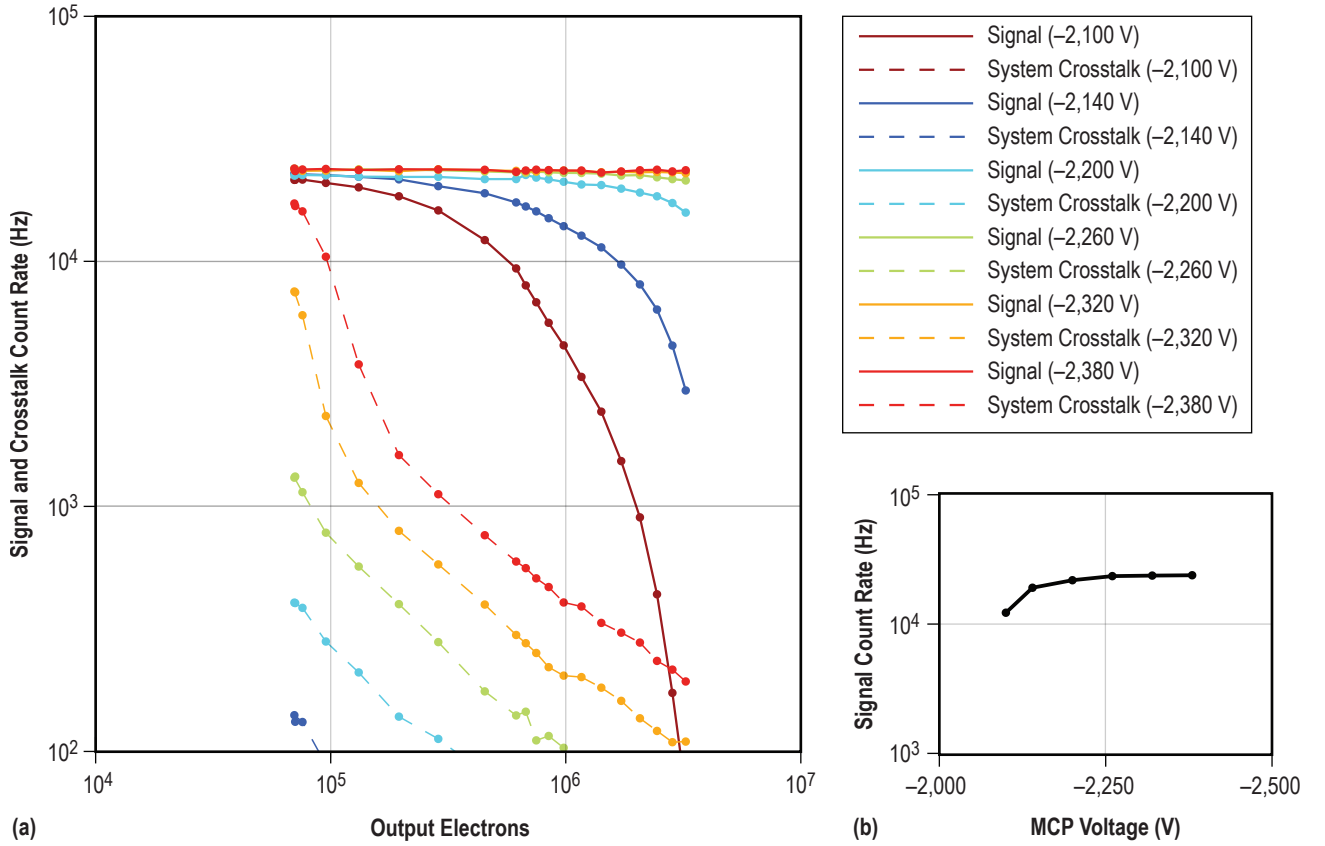


Figure 2. Example real-time plot from DIS FM14, sensor 0 detector characterization procedure for operation point determinations. The signal and crosstalk count rates are shown for 20 threshold voltages at each of 6 MCP voltages.



Figure 2 shows the typical detector characterization for DIS, in this case DIS FM14, sensor 0, pixel 11. The signal and crosstalk curves are shown at each threshold value with the crosstalk based on the average count rate of the two neighboring pixels. Figure 2(a) shows the DIS MCP threshold sweep, where count rates are plotted as a function of the nominal value of the threshold. The primary pixel, in this case, pixel 11, is used to ascertain the MCP gain and the averaged rate from the neighboring pixels of 10 and 12 are used to reveal the crosstalk characteristics. An operating voltage point was sought with the threshold close to  $4 \times 10^5$  electrons/pulse (a threshold voltage of  $\sim 2.10$  V) and a gain near  $1 \times 10^7$  electrons/pulse. At the end of each pixel's data collection, a portion of the recorded data was displayed in figure 2(b) with a single plateau curve of the signal count rate at each of the 6 MCP voltages at the constant threshold value close to  $4 \times 10^5$  electrons/pulse ( $\sim 2.10$  V). This display provided a more cursory view of an MCP operating level beyond the knee on the plateau for the pixel of the lowest gain. In the case of DIS FM14, sensor 0, shown in figure 2, the MCP operating voltage was chosen to be approximately  $-2,275$  V.

## 4.2 Energy-Azimuth Angle and Polar Angle Response

The energy and solid angle response for each pixel was determined through two separate procedures conducted for each particle energy. The first procedure provided the polar angle centroid and box-car-width (BCW) bandpass at each of the five deflected states for each illuminated pixel. The second procedure provided the coupled energy-azimuth angle response through the azimuth deflected FOV at each polar angle centroid. The resulting data from both procedures were used to derive and document all the final performance parameters for each pixel: the energy bandpass and centroids, the azimuth (deflected) angle bandpass and centroids, the polar angle bandpass and centroids, the analyzer constant, the geometric factor, and the spectrometer efficiency or effective aperture area ( $A_{eff}$ ). The effective area is defined here as the ratio of the count rate-to-input flux and includes factors such as the nonunity transmission of screens in the flight path and the nonunity efficiency of the detection system.

For reference, a BCW is equal to 1.0645 times the full width at half maximum (FWHM) and is equal to  $2.5066 \sigma$  of a Gaussian distribution. Note, in sections 4.2.1 and 4.2.2, the instrument's azimuth translates to spacecraft polar and the instrument's elevation translates to spacecraft azimuth.

### 4.2.1 Polar Angle Response

The polar response procedure enabled the determination of the centroid location and width of each pixel's polar angle bandpass. It was conducted by mechanically stepping the DIS through the 2D rotation matrix with a polar angle resolution of  $1.8^\circ$  at the centered FOV of the five deflected angles. For this procedure, the maximum count rate from the four appropriate  $V_{ESA}/V_{DEF}$  sweeps was summed for the pixel response centroid and width calculation. Figure 3(a) shows each of the 16 pixel responses at the deflected angle of  $-16.875^\circ$  along with the BCW and centroid of each pixel shown in figure 3(b). Panel (a) was displayed in real-time during the procedure with panel (b) and derived values displayed at the end of the procedure or 2D matrix. The response widths are uniform across the polar angle FOV range as shown but vary across the deflected states (not shown). This is a similar feature of all the sensors and is suggested to be due to the asymmetric effect of the deflection response, as expected, given by the axial up-down asymmetry of the optics. Figure 3 illustrates the most narrow response width viewing away from the MCP plane (up).

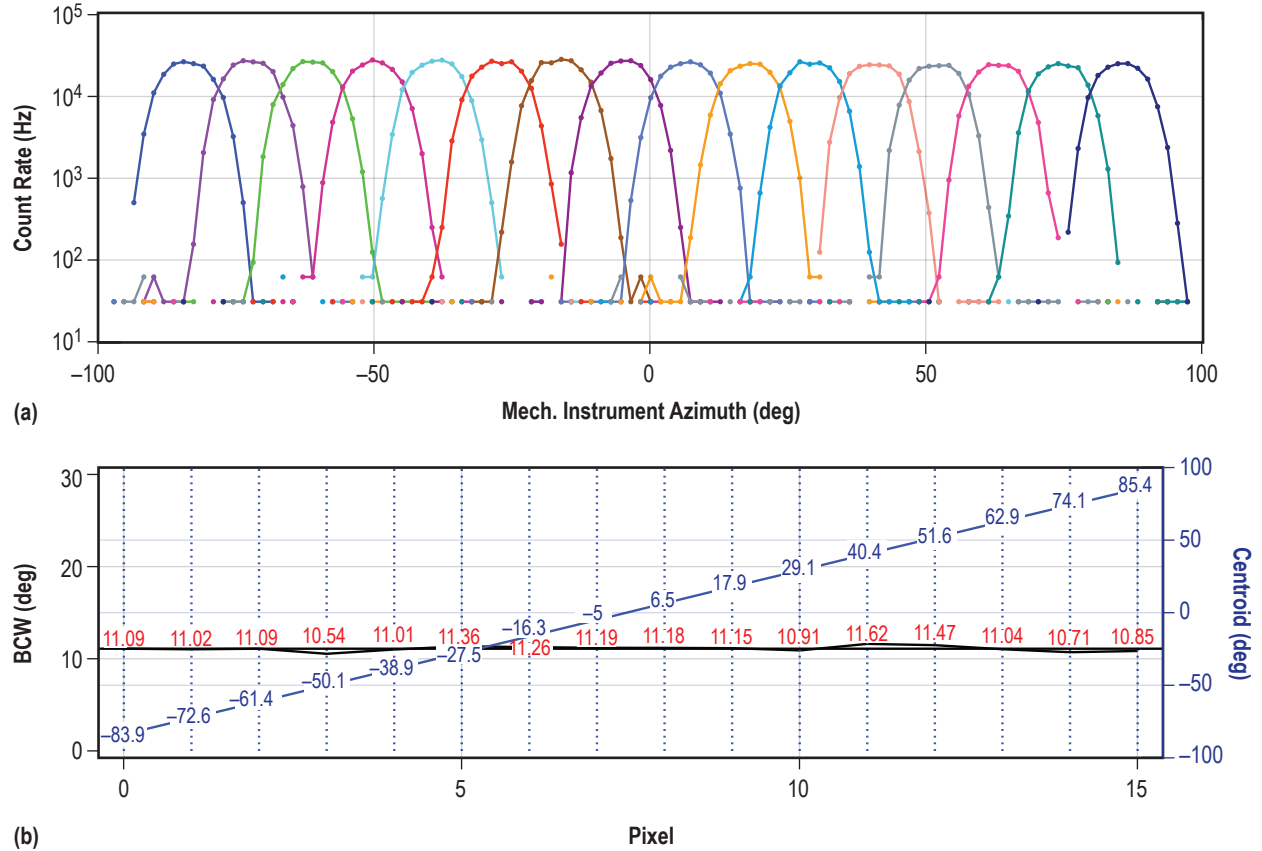


Figure 3. Example of an annotated output plot from the polar angle response procedure for DIS FM04 sensor 1. Panel (a) is plotted in real-time and shows the 16-pixel response of count rate over the full polar angle FOV at the azimuth (deflected) angle of  $-16.875^\circ$ . The lines are color coded according to pixel number. Panel (b) is plotted at the completion of the procedure documenting the centroid (right axis) and BCW (left axis) for each pixel's polar angle bandpass as shown in panel (a).

### 4.2.2 Energy-Azimuth Angle Response

The energy-azimuth angle response procedure documented the coupled energy-azimuth (deflected) angle response for each illuminated pixel and enabled the derivation of the geometric factor through the numerical integration of the energy-azimuth response functions along with the other measured values as shown in equation (1):

$$GF_{ijk} \approx \frac{\Delta\phi}{E_0^2} \sum_m \sum_n \frac{C_{ijk}}{\Phi} E_m \cos\theta_n \Delta E_m \Delta\theta_n, \quad (1)$$

where

- $G_{ijk}$  = geometric factor for pixel  $i$  at  $V_{\text{ESA}}$  step  $j$  and  $V_{\text{DEF}}$  state  $k$
- $E_m$  = energies in the energy-azimuth angle scan
- $\theta_n$  = angles in the energy-azimuth angle scan
- $\Delta E_m$  = energy resolution of the scan
- $\Delta\theta_n$  = azimuth angle resolution
- $\Delta\phi$  = polar angle resolution
- $E_0$  = energy corresponding to the response maximum in the energy-azimuth space.

This procedure was conducted by mechanically stepping the DIS aperture through the full azimuth angle FOV at a  $1.5^\circ$  resolution at the 16-pixel centroids in the polar angle FOV while synchronized with the commanded execution of the appropriate  $V_{\text{ESA}}/V_{\text{DEF}}$  stepper table for the appropriate particle energy. A few seconds after the completed procedure, marked by the end of the 2D rotation matrix, the raw analysis was completed along with the display and annotation as shown in section 4.2.2.

The 2D distributions of sensor 1 are elongated at positive azimuth angles and more circular at negative azimuths (fig. 4) and vice versa for sensor 0. This variation with deflection state primarily affects the widths for the azimuth angle bandpass as discussed in section 5.

Summing the 2D count rate maps over the energy dimension and then the azimuth angle dimension provides the 1D curves of the azimuth angle and energy ( $V_{\text{ESA}}$ ), respectively, as shown in panels (b) and (c) of figure 4. These 1D distributions were used to compute the centroids and approximate BCWs to the accuracy available through the procedure's sampling resolution. Additionally, the derived geometric factor, effective area ( $A_{\text{eff}}$ ), energy ( $dE/E$ ), azimuth ( $dEl$ ), and polar ( $dAz$ ) are annotated below panel (a) in figure 4 along with the annotated values for the analyzer constant and centroids on the right legend. (The pixel's polar angle bandpass ( $dAz$ ) is pulled from the prior polar procedure to complete the derivation of the geometric factor.) Three of the parameters are briefly discussed below.

**4.2.2.1 Analyzer Constant.** Each pixel's analyzer constant ( $eV/V$ ) was calculated from the ratio of the  $V_{\text{ESA}}$  centroid of the energy-azimuth angle response and the known particle beam energy derived from the RPA curves. This parameter increased by approximately 3% with decreasing energy and is also observed in ray-tracing results in Pollock et al.<sup>2</sup> The analyzer constant is designated as  $k$  in table 2.

**4.2.2.2 Effective Area.** Measurements of the spectrometer efficiency or the effective area ( $\text{cm}^2$ ) was calculated for each pixel and is defined here as the ratio of the peak count rate at the centroid of each 2D energy-azimuth to the input beam flux. This parameter result is annotated as  $A_{\text{eff}}$ . This performance parameter includes the nonunity transmission of screens in the particle's flight path and the nonunity efficiency of the detection system.

**4.2.2.3 Geometric Factor.** Calculation of the FPI geometric factor in units of  $\text{eV}/\text{cm}^2\text{-sr-eV}$  was performed using equation (30) of Collinson et al.<sup>7</sup> and was obtained for each illuminated pixel (16 polar angles for each of five energy-azimuth responses) for each tested particle's  $E/q$ . It is derived from the results of both the energy-azimuth and polar angle procedure and allows the determination of the differential energy flux along with the count rate per pixel measured in flight. Rigorous descriptions of the FPI pixel geometric factor derivation, appropriate techniques for its estimation using numeric particle ray tracing, its experimental determination through laboratory calibration, and its use in interpreting space plasma measurements have been provided by Collinson et al.<sup>7</sup>

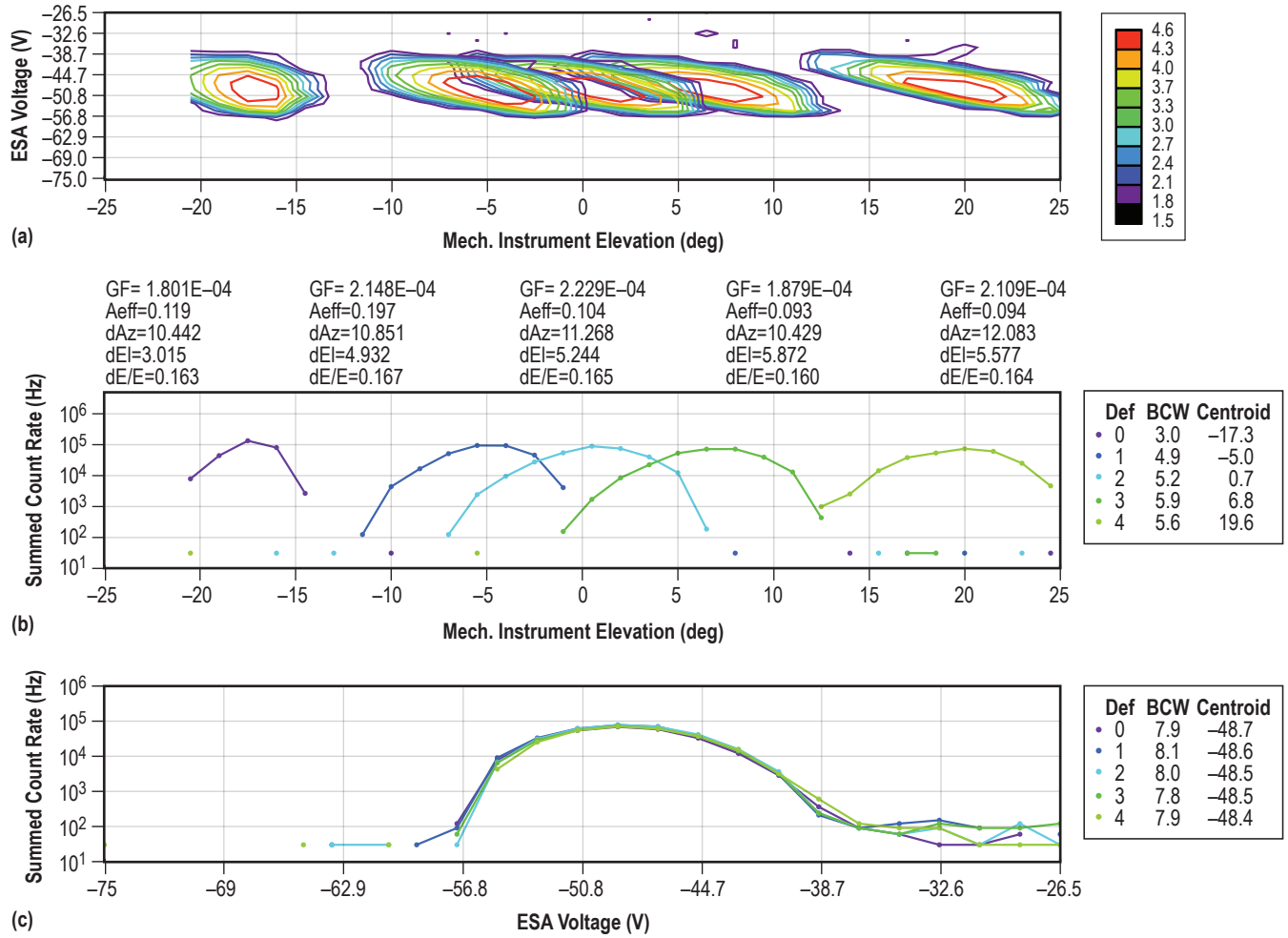


Figure 4. Near real-time graphical and tabular output from the energy-azimuth angle procedure of 250 eV in the case of DIS FM16, sensor 1, pixel 2. Panel (a) shows the 2D energy-azimuth angle count rate response at five deflection states at the nominally centered angles of  $-16.875^\circ$ ,  $-5.625^\circ$ ,  $0^\circ$ ,  $5.625^\circ$ , and  $16.875^\circ$ . The horizontal axis label of instrument elevation translates to spacecraft azimuth. Panel (b) shows the 1D azimuth responses, and panel (c) shows the 1D energy ( $V_{ESA}$ ) responses. The curves in panels (b) and (c) are color coded according to the deflection state along with the response widths and centroids that are annotated on the right. Also shown are the derived values of the geometric factor, the effective area ( $A_{eff}$ ), polar angle width ( $dAz$ ), azimuth angle width ( $dEl$ ), and energy resolution ( $dE/E$ ) for each deflected state. The response centered near  $-16.875^\circ$  is cut off at higher angles due to a hardware limit in the chamber and so gives artificially smaller performance values.

## 5. SUMMARY RESULTS

Table 2 summarizes the important performance parameters and their variability as measured in the calibration laboratory for a 3 keV  $E/q$  particle beam. The values and uncertainties are given as mean values and standard deviations based on the independent measurements across 16 DISs  $\times$  2 sensors  $\times$  16 pixels. These are tabulated for each of the four flight deflection states in addition to the undeflected state. An exception is that results from the heavily truncated counts distributions discussed in the context of figure 4 (truncation near  $-20^\circ$ ) are not included in these calculations. The factors  $k$  and  $k_{\text{DEF}}$  are the analyzer and deflection constants, respectively, and are defined in their respective row headings. The values in table 2 are consistent with those based on numerical ray tracing in figure 35 of Pollock et al.<sup>2</sup>

Table 2. Calibration measured performance.

	Down 16.875°		Down 5.625°		0°		Up 5.625°		Up 16.875°	
	Mean	Std. Dev.	Mean	Std. Dev.	Mean	Std. Dev.	Mean	Std. Dev.	Mean	Std. Dev.
$k_e (E/qV_e)$	5.10	0.08	5.08	0.06	5.10	0.06	5.06	0.06	5.06	0.06
$\delta\epsilon/\epsilon$	0.121	0.005	0.126	0.004	0.126	0.004	0.126	0.004	0.124	0.004
$k_\phi (V_{\text{DEF}}/\theta/V_e)$	0.045	0.0005	0.044	0.0009	NA	NA	0.046	0.0008	0.046	0.0005
$\Delta\phi$ (FWHM)	5.78	0.25	5.67	0.31	5.44	0.31	4.70	0.34	2.94	0.51
$\delta\theta$ (BCW)	14.6	1.9	12.7	0.8	12.3	0.8	12.3	0.7	11.8	0.7
$G$ (cm <sup>2</sup> -sr-eV/eV)	0.00020	0.00007	0.00021	0.00008	0.00021	0.00008	0.00020	0.00007	0.00016	0.00006

### 5.1 Variation Across Deflection States

In the column headings of table 2 that define the deflection state, the words ‘Down’ and ‘Up’ are shown where down means viewing toward the plane of the MCP and up means viewing away from the MCP plane. The decreasing width in the azimuth response as the look direction proceeds from downward to upward is evident. This effect is observed in both calibration and ray-tracing results as discussed in Pollock et al.<sup>2</sup> A decreasing width in the polar angle response across deflection states is also observed in the same direction from down to up. It is suggested that this variation is due to the same asymmetry in the deflection optics as it was for the energy-azimuth response as discussed in Pollock et al.<sup>2</sup> and Collinson et al.<sup>7</sup>

### 5.2 Variation Across Energy/Charge

The  $\delta\epsilon/\epsilon$  (also designated as  $dE/E$ ) bandpass measured in calibration increased for low energies due to two reasons: the field penetration from the MCP stack into the exit of the ESA as discussed in Pollock et al.<sup>2</sup> and the increasing temperature of the input beam with lower energies. In a later study of several low-energy procedures, the beam width was removed from the measured DIS

$\delta\epsilon/\epsilon$  width with the revised bandpass being within 5% of the predicted ray-traced results. The beam width was obtained from the procedure's RPA curve analysis and removed by applying a simple root mean square sum method. A calibration result that is not consistent with the ray-tracing results is an energy dependence observed in the deflection response,  $k_{\text{DEF}}$ , at low energies. This is being further studied for its possible cause in the facility, in the flight data, and 3D ray tracing.

## 6. CONCLUSIONS AND LESSONS LEARNED

Two observations can be made from the DIS performance summary values in table 2. The tight precision of the DIS ESA gap of 4.5 mm was needed to meet the FPI requirements for the mission objectives. Precision machining and insulator pin alignment were used to achieve this gap across the entire toroidal ESA and among all the ESAs to achieve a uniform response at all polar and azimuth look directions across the DIS spectrometer set. Moreover, a methodical calibration with the required sampling and precision was needed, and this being done, did allow the determination of uniformities across the set and any nonuniformities within the set.

There were lessons learned from this calibration task due to a combination of factors, namely, the large number of instrument sensors involved, the tight schedule, and its long duration. Prior to the calibration start, additional time with the engineering unit would have been ideal to characterize and resolve instrument design and performance issues, and further develop test processes and procedures. More than 32 flight sensors ( $16 \times 2$ ) were calibrated in the short timeframe of 52 weeks. This presented challenges that resulted in necessary management practices across the three located groups. As the flight units were sequentially built and environmentally tested by Meisei Electric and ISAS, it was important that the calibration of each unit followed.

During the task duration, two instruments were delivered for calibration as the next two were completing their build and environmental testing. There were no delays between the exit of one instrument and the chamber mounting of another so habitual behaviors became important. Most importantly, focus, fatigue, and complacency were foremost in team members' minds and monitored continuously by all during the arduous task. Monitoring during the procedures of the three real-time displays of housekeeping, varying parameters, and their associated dependent count rate was necessary to immediately detect anomalies. A daily review allowed a continuous knowledge base so that any arising instrumental issues could be handled promptly to minimize delays.

For this review, the completed analysis of each unit's performance results was delivered and discussed with the team the following morning. The team then held a summary review of all the instruments' completed analysis before the unit was swapped in the chamber for the next one. Ideally, there would be at least a full day between the completion of the calibration and the summary review. Administratively, each unit's as-run documentation was extensive from the time of entrance through exit. It was important that all files produced from the automated procedures from each of the three software functions had the same time-stamped filenames but with different suffixes, depending on its software origin. Finally, these same ASCII and PDF plots were extensively annotated with the unit, the sensor, all voltage settings, stepper table, software version numbers, procedure time stamp, and printed time stamp, along with the completed raw analysis values.



## REFERENCES

1. Young, D.T.; Bame, S.J.; Thomsen, M.F.; et al.: “ $2\pi$  radian field-of-view toroidal electrostatic analyzer,” *Rev. Sci. Instrum.*, Vol. 59, No. 5, pp. 743–751, doi: 10.1063/1.1139821, 1988.
2. Pollock, C.; Moore, T.; Jacques, A.; et al.: “Fast Plasma Investigation for Magnetospheric MultiScale,” *Space Sci. Rev.*, Vol. 199, No. 1, pp. 331–406, 2016.
3. Biddle, A.P.; and Reynolds, J.M.: “Integrated development facility for the calibration of low-energy charged particle flight instrumentation,” *Rev. Sci. Instrum.*, Vol. 57, No. 4, p. 572, doi: 10.1063/1.1138873, 1986.
4. Valek, P.W.: “Development of spacecraft borne instrumentation and analysis of low energy outflow,” Ph.D. Thesis, Auburn University, Auburn, AL, 2001.
5. Funsten, H.O.; Harper, R.W.; and McComas, D.J.: “Absolute detection efficiency of space-based ion mass spectrometers and neutral atom imagers,” *Rev. Sci. Instrum.*, Vol. 76, 053301, doi: <http://dx.doi.org/10.1063/1.1889465>, pp. 053301-1 through 053301-4, 2005.
6. Gliese, U.; Avanov, L.A.; Barrie, A.; et al.: “New Method for Accurate Calibration of Micro-Channel Plate based Detection Systems and its use in the Fast Plasma Investigation of NASA’s Magnetospheric Multiscale Mission,” abstract SM11B-2095 presented at 2013 Fall Meeting, *AGU*, San Francisco, CA, 2013.
7. Collinson, G.A.; Dorelli, J.C.; Avanov, L.A.; et al.: “The geometric factor of electrostatic plasma analyzers: A case study from the Fast Plasma Investigation for the Magnetospheric Multiscale Mission,” *Rev. Sci. Instrum.*, Vol. 83, 033303, doi: 10.1063/1.3687021, pp. 033303-1 through 033303-10, 2012.

REPORT DOCUMENTATION PAGE				Form Approved OMB No. 0704-0188	
<p>The public reporting burden for this collection of information is estimated to average 1 hour per response, including the time for reviewing instructions, searching existing data sources, gathering and maintaining the data needed, and completing and reviewing the collection of information. Send comments regarding this burden estimate or any other aspect of this collection of information, including suggestions for reducing this burden, to Department of Defense, Washington Headquarters Services, Directorate for Information Operation and Reports (0704-0188), 1215 Jefferson Davis Highway, Suite 1204, Arlington, VA 22202-4302. Respondents should be aware that notwithstanding any other provision of law, no person shall be subject to any penalty for failing to comply with a collection of information if it does not display a currently valid OMB control number.</p> <p><b>PLEASE DO NOT RETURN YOUR FORM TO THE ABOVE ADDRESS.</b></p>					
1. REPORT DATE (DD-MM-YYYY) 01-04-2017		2. REPORT TYPE Technical Publication		3. DATES COVERED (From - To)	
4. TITLE AND SUBTITLE  Dual Ion Spectrometers and Their Calibration for the Fast Plasma Investigation on NASA's Magnetospheric Multiscale Mission				5a. CONTRACT NUMBER	
				5b. GRANT NUMBER	
				5c. PROGRAM ELEMENT NUMBER	
6. AUTHOR(S)  V.N. Coffey and M.O. Chandler				5d. PROJECT NUMBER	
				5e. TASK NUMBER	
				5f. WORK UNIT NUMBER	
7. PERFORMING ORGANIZATION NAME(S) AND ADDRESS(ES) George C. Marshall Space Flight Center Huntsville, AL 35812				8. PERFORMING ORGANIZATION REPORT NUMBER  M-1429	
9. SPONSORING/MONITORING AGENCY NAME(S) AND ADDRESS(ES) National Aeronautics and Space Administration Washington, DC 20546-0001				10. SPONSORING/MONITOR'S ACRONYM(S)  NASA	
				11. SPONSORING/MONITORING REPORT NUMBER NASA/TP-2017-218237	
12. DISTRIBUTION/AVAILABILITY STATEMENT Unclassified-Unlimited Subject Category 88 Availability: NASA STI Information Desk (757-864-9658)					
13. SUPPLEMENTARY NOTES  Prepared by the Spacecraft & Vehicle Systems Department, Engineering Directorate					
14. ABSTRACT The scientific target of NASA's Magnetospheric Multiscale (MMS) mission is to study the fundamentally important phenomenon of magnetic reconnection. Theoretical models of this process predict a small size, on the order of hundred kilometers, for the ion diffusion region where ions are demagnetized at the dayside magnetopause. This region may typically sweep over the spacecraft at relatively high speeds of 50 km/s, requiring the fast plasma investigation (FPI) instrument suite to have an extremely high time resolution for measurements of the 3D particle distribution functions. As part of the FPI on MMS, the 16 dual ion spectrometers (DIS) will provide fast (150 ms) 3D ion velocity distributions, from 10 to 30,000 eV/q, by combining the measurements from four dual spectrometers on each of four MMS spacecraft. For any multispacecraft mission, the response uniformity among the spectrometer set assumes an enhanced importance. Due to these demanding instrument requirements and the effort of calibrating more than 32 sensors (16x2) within a tight schedule, a highly systematic and precise calibration was required for measurement repeatability. To illustrate how this challenge was met, a brief overview of the FPI DIS was presented with a detailed discussion of the calibration method of approach and implementation. Finally, a discussion of DIS performance results, their unit-to-unit variation, and the lessons learned from this calibration effort are presented.					
15. SUBJECT TERMS space, plasma, magnetospheric, instrumentation, calibration, testing					
16. SECURITY CLASSIFICATION OF:			17. LIMITATION OF ABSTRACT  UU	18. NUMBER OF PAGES 28	19a. NAME OF RESPONSIBLE PERSON STI Help Desk at email: help@sti.nasa.gov
a. REPORT U	b. ABSTRACT U	c. THIS PAGE U			19b. TELEPHONE NUMBER (Include area code) STI Help Desk at: 757-864-9658



National Aeronautics and  
Space Administration  
IS02

**George C. Marshall Space Flight Center**  
Huntsville, Alabama 35812